Molecular Cell
Article

A Conformational Switch in Bacteriophage P22 Portal Protein Primes Genome Injection

Hongjin Zheng,[1] Adam S. Olia,[2] Melissa Gonen,[1] Simeon Andrews,[1] Gino Cingolani,[2,*] and Tamir Gonen[1,*]
[1]Department of Biochemistry, University of Washington, 1705 NE Pacific Street, Seattle, WA 98195, USA
[2]Department of Biochemistry and Molecular Biology, State University of New York Upstate Medical University, 750 East Adams Street, Syracuse, NY 13210, USA
*Correspondence: tgonen@u.washington.edu (T.G.), cingolag@upstate.edu (G.C.)
DOI 10.1016/j.molcel.2007.11.034

SUMMARY

Double-stranded DNA (dsDNA) viruses such as herpesviruses and bacteriophages infect by delivering their genetic material into cells, a task mediated by a DNA channel called "portal protein." We have used electron cryomicroscopy to determine the structure of bacteriophage P22 portal protein in both the procapsid and mature capsid conformations. We find that, just as the viral capsid undergoes major conformational changes during virus maturation, the portal protein switches conformation from a procapsid to a mature phage state upon binding of gp4, the factor that initiates tail assembly. This dramatic conformational change traverses the entire length of the DNA channel, from the outside of the virus to the inner shell, and erects a large dome domain directly above the DNA channel that binds dsDNA inside the capsid. We hypothesize that this conformational change primes dsDNA for injection and directly couples completion of virus morphogenesis to a new cycle of infection.

INTRODUCTION

The icosahedral capsid represents a formidable example of a biological nanocage that withstands tremendous internal pressures generated by the tightly packaged viral genome (Chemla et al., 2005; Ivanovska et al., 2004; Johnson and Chiu, 2007). In many bacteriophages and herpesviruses, the capsid displays extraordinary structural plasticity and undergoes dramatic conformational changes during viral maturation (Jiang et al., 2003; Johnson and Chiu, 2007; Knopf, 2000; Mettenleiter et al., 2006; Steven et al., 1997; Zhang et al., 2000). In the morphogenesis of the double-stranded DNA (dsDNA) bacteriophage P22, a well-characterized member of the Podovirus family, the coat protein (gp5), together with scaffolding (gp8), portal protein (gp1), and injection proteins (gp7, gp17, gp20), self-assembles to form a 600 Å spherical intermediate known as the procapsid (Israel, 1977; Jiang et al., 2003; Johnson and Chiu, 2007; Thuman-Commike et al., 1996; Zhang et al., 2000). The portal protein occupies a unique vertex of the icosahedron, where it forms a gateway through the proteinaceus capsid as well as the attachment site for external tail accessory factors. The terminase complex (gp2, gp3) temporarily associates with portal protein to form the "genome packaging motor," a powerful molecular machine that uses ATP to package dsDNA into the capsid (Casjens and Huang, 1982; Jackson et al., 1982). While the viral genome is packaged inside the virion (Casjens and Huang, 1982; Earnshaw and Harrison, 1977; Earnshaw et al., 1978; Jackson et al., 1982), the capsid volume increases 2-fold through major conformational changes in coat proteins (Jiang et al., 2003; Thuman-Commike et al., 1996; Zhang et al., 2000) and becomes an angularized icosahedron more than 700 Å in diameter (Chang et al., 2006). Finally, the terminase complex dissociates from portal protein, and the "genome injection machinery" begins to assemble in preparation for a new cycle of viral infection (Johnson and Chiu, 2007).

During infection, the viral genome is injected through the portal protein channel into the host. In P22, the genome injection machinery is a 2.8 mDa molecular machine composed of a dodecamer of gp1 (Chang et al., 2006; Lander et al., 2006) forming the portal protein, in complex with several copies of tail accessory factors gp4, gp10, and gp26, which assemble sequentially onto portal protein in this order (Bhardwaj et al., 2007; Strauss and King, 1984). This is followed by the attachment of the tailspike adhesin gp9, which completes the assembly of the genome injection machinery, rendering the virus fully infectious (Chang et al., 2006; Johnson and Chiu, 2007; Lander et al., 2006).

Using electron cryomicroscopy, we show that portal protein undergoes dramatic quaternary structure rearrangements during virus maturation. We propose that, similarly to the coat protein, the portal protein adopts a procapsid conformation and a mature phage conformation. The mature phage conformation, which is induced by gp4 binding, enables portal protein to bind viral DNA and likely recruits the injection proteins inside the virion in preparation for a new cycle of viral infection.

RESULTS AND DISCUSSION

Procapsid Form of Dodecameric Portal Protein

Portal protein from bacteriophage P22 is significantly larger than in most phages (~1 mDa) and is therefore more similar to portals found in the herpesvirus family (Newcomb et al., 2001). Ectopically expressed P22 portal protein is polymorphic in solution, consisting of rings of 11- and 12-fold symmetry (Cingolani et al., 2002; Lander et al., 2006; Orlova et al., 2003; Poliakov

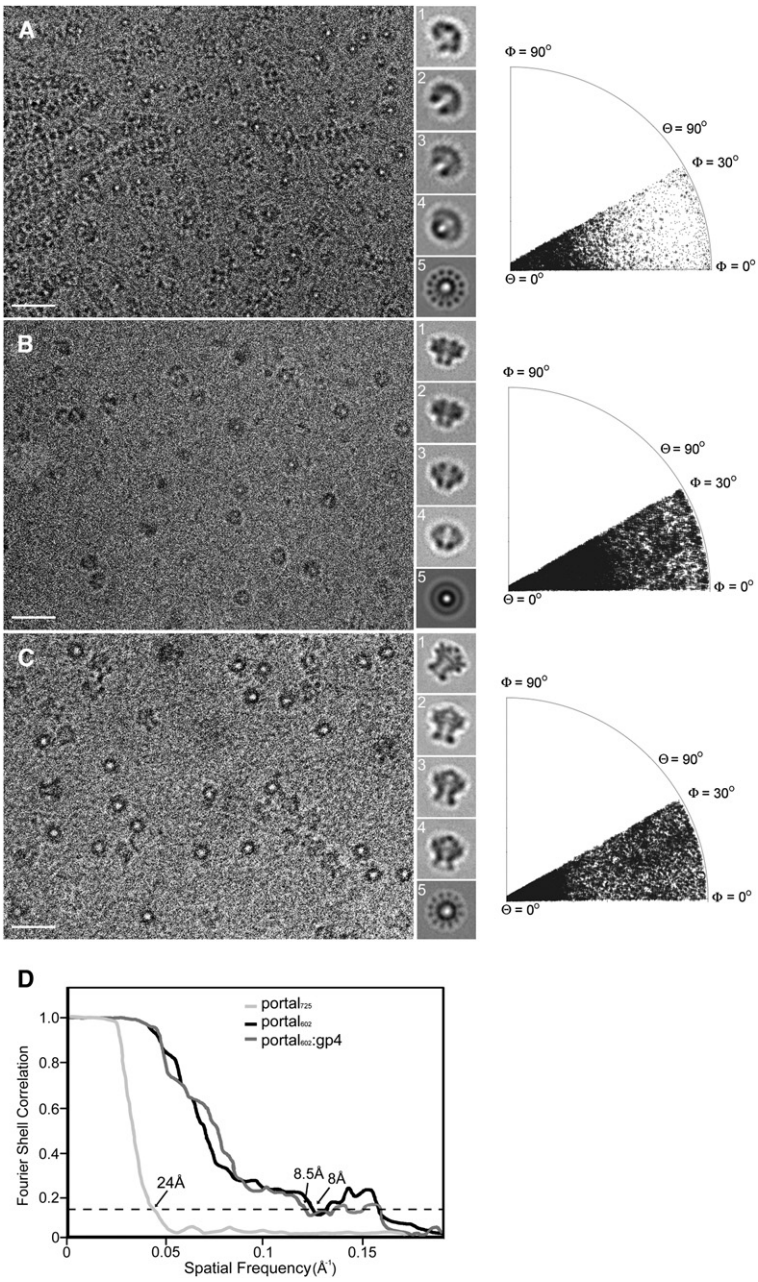

Figure 1. Electron Cryomicroscopic Analysis of 12-Fold Symmetric Assemblies of Portal$_{725}$, Portal$_{602}$, and Portal$_{602}$:gp4

(A–C) Representative electron cryomicroscopy micrographs for portal$_{725}$, portal$_{602}$, and portal$_{602}$:gp4 complexes, respectively. Projection averages are shown in the middle and angular distribution plots on the right.

(A) Portal$_{725}$ particles form many head-to-head or head-to-tail interactions, limiting the usefulness of this preparation for structural analysis. Note the paucity of side views.

(B) Portal$_{602}$ distributes more evenly on the cryomicroscopy grid and is therefore a far better cryomicroscopy sample than portal$_{725}$.

(C) Portal$_{602}$:gp4 complexes. Side-view projection averages show an elongated particle when compared with portal$_{602}$. A strong density above the crown domain resembling a cap is seen. Twelve spokes are clearly visible in top view projection averages, indicating that dramatic conformational changes in portal protein ensue following gp4 binding.

(D) The resolutions for all reconstructions were determined using the 0.143 (Rosenthal and Henderson, 2003) criteria and are indicated in the plot as 24 Å for portal$_{725}$, 8.5 Å for portal$_{602}$:gp4, and 8 Å for portal$_{602}$. Scale bar, 30 nm. The size length of individual projection average boxes is 20 nm.

et al., 2007). We developed a purification protocol that yields a homogeneous preparation of dodecameric rings (Lorenzen et al., 2008) and analyzed the structure of portal protein by electron cryomicroscopy (Figure 1). Notably, full-length portal protein (portal$_{725}$) displayed a biased orientation on cryogrids, which was complicated by the tendency of the protein to form elongated aggregates (Figure 1A). Due to the paucity of side views (De Rosier and Klug, 1968), only a low-resolution 3D model of the portal$_{725}$ was reconstructed from frozen hydrated particles (see Figure S1 available online). However, a carboxy-terminal truncation of portal protein spanning only residues 1–602, and called "portal$_{602}$," behaved as an ideal specimen for cryomicroscopy (Figure 1B). Portal$_{602}$ has hydrodynamics, oligomerization properties, and biochemical binding activity identical to the full-length portal (Figure S2). Native mass spectrometry confirms that portal$_{602}$ assembles exclusively into stable 12-mers (Lorenzen et al., 2008). In vivo, the carboxy-terminal end of portal protein is dispensable for oligomerization (Lorenzen et al., 2008), assembly into the virion, and virus infectivity (Bazinet et al., 1990). A 3D reconstruction of portal$_{602}$ is shown in Figure 2. The quaternary structure of dodecameric portal$_{602}$ resembles a hollow mushroom, 155 Å in diameter and 110 Å tall with a central pore 35 Å in diameter, large enough to accommodate fully hydrated dsDNA. Similar overall architecture has been reported for portal proteins from other viruses such as herpesvirus, Phi 29, SPP1, and T7 (Agirrezabala et al., 2005; Guasch et al., 1998; Orlova et al., 2003; Simpson et al., 2000; Trus et al., 2004). Three distinct domains are identified in side view, annotated from top to bottom as the collar, crown, and funnel domains (Figure 2A). The "top" of the portal protein is the region that resides inside the virion (Chang et al., 2006; Lander et al., 2006), while the "bottom" is the region that protrudes outwards. Directly below the collar domain, the crown domain consists of 12 clearly defined spokes emanating from the central DNA channel in portal$_{725}$ (Figure S1), which appear truncated in portal$_{602}$ (Figures 1A, 1B, and 2C and Figure S1E). The spokes have a periodicity of 30° and adopt a slightly anticlockwise orientation when viewed from the top (Figure S1). The funnel domain is 45 Å long, is 80 Å in diameter, and is situated directly below the crown domain. It protrudes away from the viral capsid and forms the only possible interface between portal protein and adaptor proteins such as the terminase complex or the tail accessory factor gp4 (Chang et al., 2006; Johnson and Chiu, 2007; Lander et al., 2006).

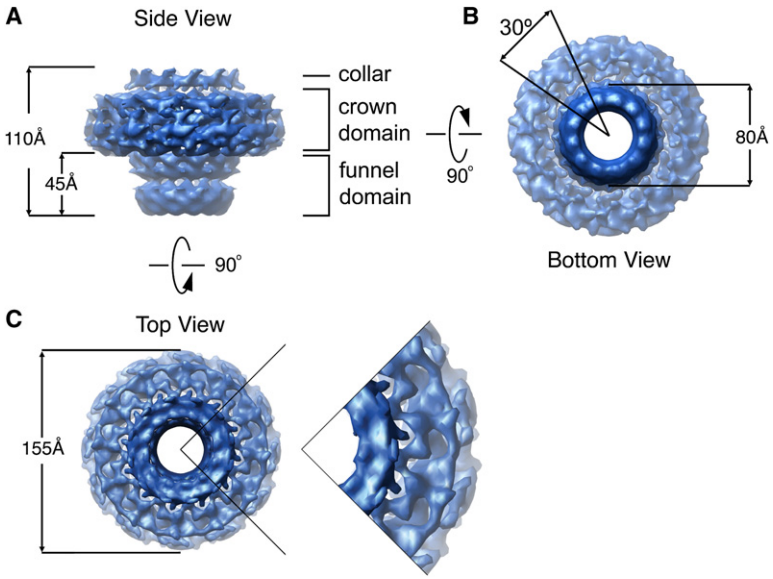

Figure 2. Structure of 12-Fold Symmetric Portal$_{602}$ at 10 Å Resolution

Electron cryomicroscopy structure of portal$_{602}$ in the procapsid form. For all figures, we define the "top" as the region of portal that would reside inside the P22 virion, while the "bottom" is the region that would protrude outward.

(A) In side view, the portal assembly adopts a mushroom-like conformation of about 110 Å in height, which presents three domains, annotated from top to bottom as the collar, crown, and funnel domains.

(B and C) Bottom and top views of dodecameric portal$_{602}$ ring reveal a central pore large enough to accommodate hydrated dsDNA. The outer diameters of the crown and funnel domains are approximately 155 and 80 Å, respectively. In all panels, the density map was normalized using MAPMAN (Kleywegt and Jones, 1996) and displayed at a contour level of 4.6σ above background corresponding to the molecular mass as calculated in SPIDER (Frank et al., 1996).

Mature Capsid Form of Dodecameric Portal$_{602}$ in Complex with gp4

The funnel domain of the portal protein protrudes out from the viral capsid, leaving it as the only possible binding site for gp4 (Chang et al., 2006; Lander et al., 2006). In our cryomicroscopy reconstructions, gp4 binds to the funnel domain of portal$_{602}$ in a one-to-one ratio (Figure S2), in full agreement with previously published data (Olia et al., 2006). The density corresponding to gp4 is represented by two 12-fold symmetric concentric rings, which are consistent with a total mass of ~220 kDa and correspond to 12 copies of gp4 (Figure 3A, dashed box). In the gp4-bound form, portal$_{602}$ undergoes dramatic conformational changes spanning the entire length of the channel (Figure 3A). The funnel domain increases in diameter from 85 to 110 Å while the crown domain reconfigures, now displaying 12 well-defined spokes (Figures 3B and 3C). The collar domain decreases its diameter from 85 to 70 Å in the portal$_{602}$:gp4 complex and exposes 12 elongated rod-like densities pointing straight up toward a large dome, 40 Å in diameter, that is situated directly above the DNA channel (Figure 3A).

The density of the dome domain may originate from regions of portal$_{602}$ that are disordered in the procapsid form of portal protein, and therefore invisible in our 3D reconstructions, but become stabilized following gp4 binding. Although the density

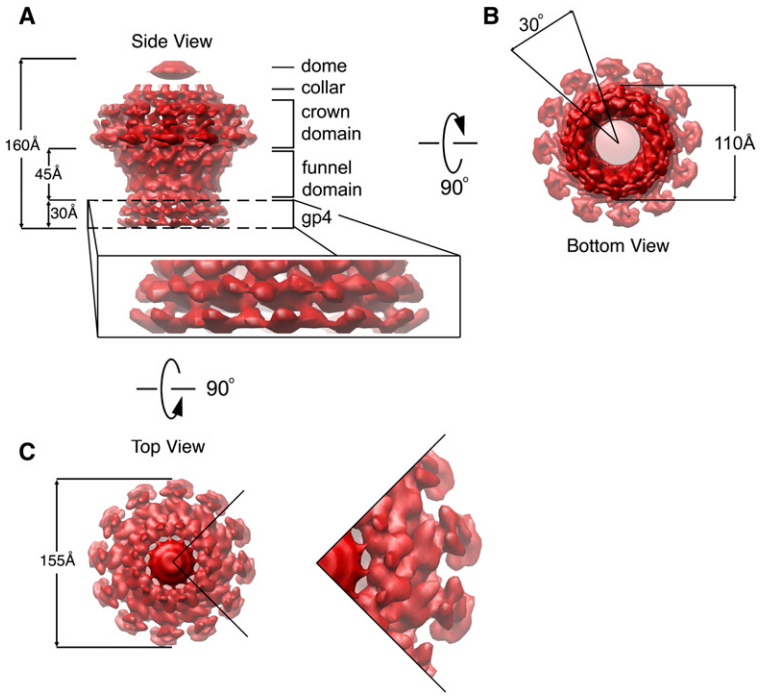

Figure 3. Structure of 12-Fold Symmetric Portal$_{602}$:gp4 Complex at 10 Å Resolution

Electron cryomicroscopy structure of portal$_{602}$ bound to twelve copies of gp4.

(A) (Side view) The portal$_{602}$:gp4 complex is 160 Å in height. The gp4 density is visible directly below the funnel domain and contributes 30 Å to the total height of the complex (enlarged box). A large dome-shaped domain is seen above the collar domain, directly over the pore of the DNA channel.

(B and C) Bottom and top views of portal$_{602}$:gp4 complex reveal that, following gp4 binding, the central DNA channel remains hollow but is occluded by a large dome-shaped domain at the very top. The overall diameter of the crown domain remains unchanged from portal$_{602}$ at 155 Å but now presents 12 clearly defined spokes. The funnel domain increases its diameter to 110 Å. As for Figure 2, the density map for portal$_{602}$:gp4 complex was filtered to 10 Å, normalized using MAPMAN (Kleywegt and Jones, 1996), and displayed at 4.1σ above background corresponding to the molecular mass as calculated in SPIDER (Frank et al., 1996).

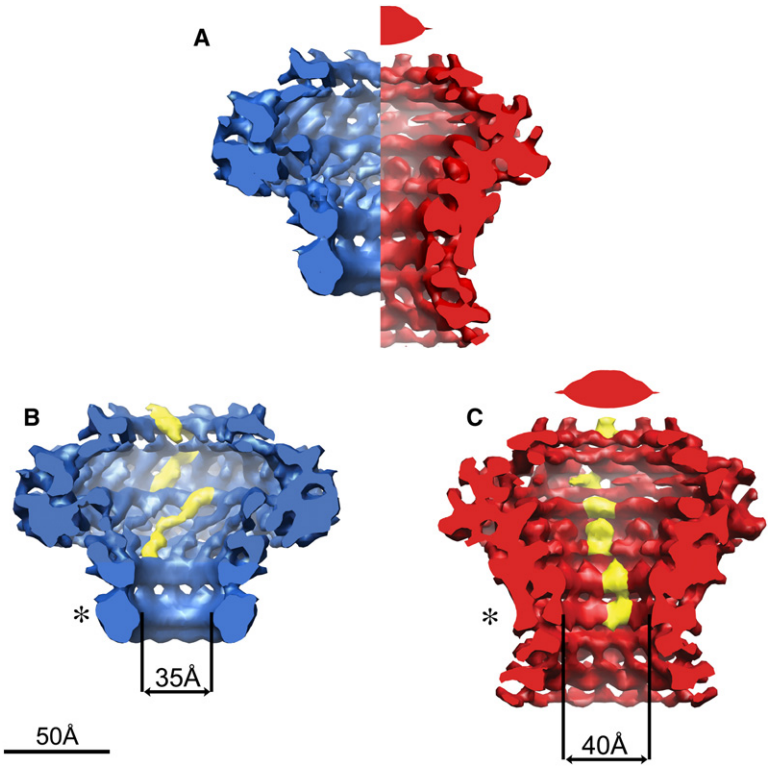

Figure 4. Gp4 Induces Dramatic Conformational Changes in the Portal$_{602}$ DNA Channel

(A) Comparable sliced side views of portal$_{602}$ (blue) and portal$_{602}$:gp4 (red) filtered to identical resolution (10 Å) and displayed at 4.6σ and 4.1σ above background, respectively. Gp4 binding to the funnel domain triggers an overall reorganization of the internal features of the DNA channel.

(B) Sliced side view of portal$_{602}$ identifies the funnel domain as the narrowest point in the DNA channel at 35 Å diameter (asterisk). Cylindrical densities line the channel pore in a zig-zag fashion (yellow highlights).

(C) Sliced side view of portal$_{602}$:gp4 complex. The funnel domain increases slightly in diameter to 40 Å but still represents the narrowest point in the DNA channel (asterisk). Pore-lining densities no longer adopt a zig-zag orientation but rather appear to be pointing straight toward the center of the channel (yellow highlights).

of the dome seems discontinuous from the portal$_{602}$:gp4 complex (Figure 3A), at a lower contour level (2.9σ above background), the density is continuous, suggesting that the dome is connected to the collar domain of portal$_{602}$ by flexible loops. Overall, the binding of gp4 to the funnel domain of portal$_{602}$ induces a conformational change that is transmitted over 100 Å away, from a location outside of the viral capsid to the inner DNA-filled cavity (Chang et al., 2006; Lander et al., 2006).

The internal structure of portal$_{602}$ undergoes dramatic conformational changes upon gp4 binding. As seen in a side-view slice through the DNA channel of portal protein, the channel diameter ("vestibule") changes, and pore-lining densities reorient (Figure 4). Prior to gp4 binding, the funnel domain forms the constriction site in the channel with a diameter of 35 Å (Figure 4B, asterisk). Directly above, the vestibule opens up in the crown domain to a diameter of 70 Å and finally narrows again at the collar to 40 Å. Pore-lining densities in portal$_{602}$ are elongated, appear rod-like in shape, and are tilted with respect to the vertical axis of the portal protein (Figure 4B, yellow highlights). Following gp4 binding to portal$_{602}$, both the channel diameter and the orientation of the pore-lining densities change. The channel diameter widens to 40 Å at the constriction site (Figure 4C, asterisk), 80 Å at the crown domain, and 45 Å at the collar. Most dramatically, all pore-lining densities reorient perpendicularly to the vertical axis of the pore and appear to point straight inwards toward the center of the DNA channel (Figure 4C, yellow highlights).

The Dome Is a DNA Scaffolding Domain

Incubation of portal$_{602}$:gp4 with a 38-mer dsDNA oligonucleotide (~130 Å in length) clearly revealed DNA bound to the dome domain in negatively stained preparations (Figure 5A, arrows). Portal$_{602}$ did not bind DNA in the absence of gp4 (data not shown), suggesting that conformational changes induced by gp4 binding not only stabilize the dome domain but also prime this molecular machinery for binding DNA.

How does the dome bind DNA? Sequence alignment of nine portal proteins identified a single conserved motif of positively charged residues, ^{286}KRRR^{289}, common to all members of the Podoviridae family of bacteriophages (Figure 5B, yellow). This region is disordered in the structure of Phi 29 portal protein, where it was thought to form part of the collar domain and project into the DNA channel (Guasch et al., 1998; Simpson et al., 2001; Simpson et al., 2000). Secondary structure prediction for the P22 portal protein suggests that this motif falls in a region (residues 277–293) with high propensity to fold into a helix, which we will refer to as DNA-binding helix or "db helix." Overall, the db helix contains seven positively charged residues that may be important for DNA binding (Figure 5B). A helical wheel representation of the db helix reveals diametrically opposed positively charged and hydrophobic faces (Figures 5C and 5D). Side-by-side packing of 12 such db helices within the dome domain would create a tunnel lined with strong positive surface charge that could be important for binding DNA. In this scenario, the positively charged residues are important for binding DNA and could be used to chaperone DNA through the channel, while the hydrophobic face could be used for helix-helix packing interactions that stabilize the dome domain.

We hypothesize that the db helix is disordered in the procapsid conformation of portal protein but becomes structured in the mature capsid form following gp4 binding. Polyarginine repeats have been previously reported to have an intrinsic structural plasticity. For instance, the arginine-rich RRE-binding element of HIV-1 Rev protein is fully helical in complex with a 35-mer RRE RNA aptamer I (Ye et al., 1996), whereas it adopts an extended conformation (Ye et al., 1999) in complex with the 27-mer RRE RNA aptamer II. The transition between the two structural forms presumably occurs upon interaction with the acidic RNA pocket. Similarly, the IBB domain of importin α also presents a basic stretch, ^{28}RRRR^{31}, which adopts a random

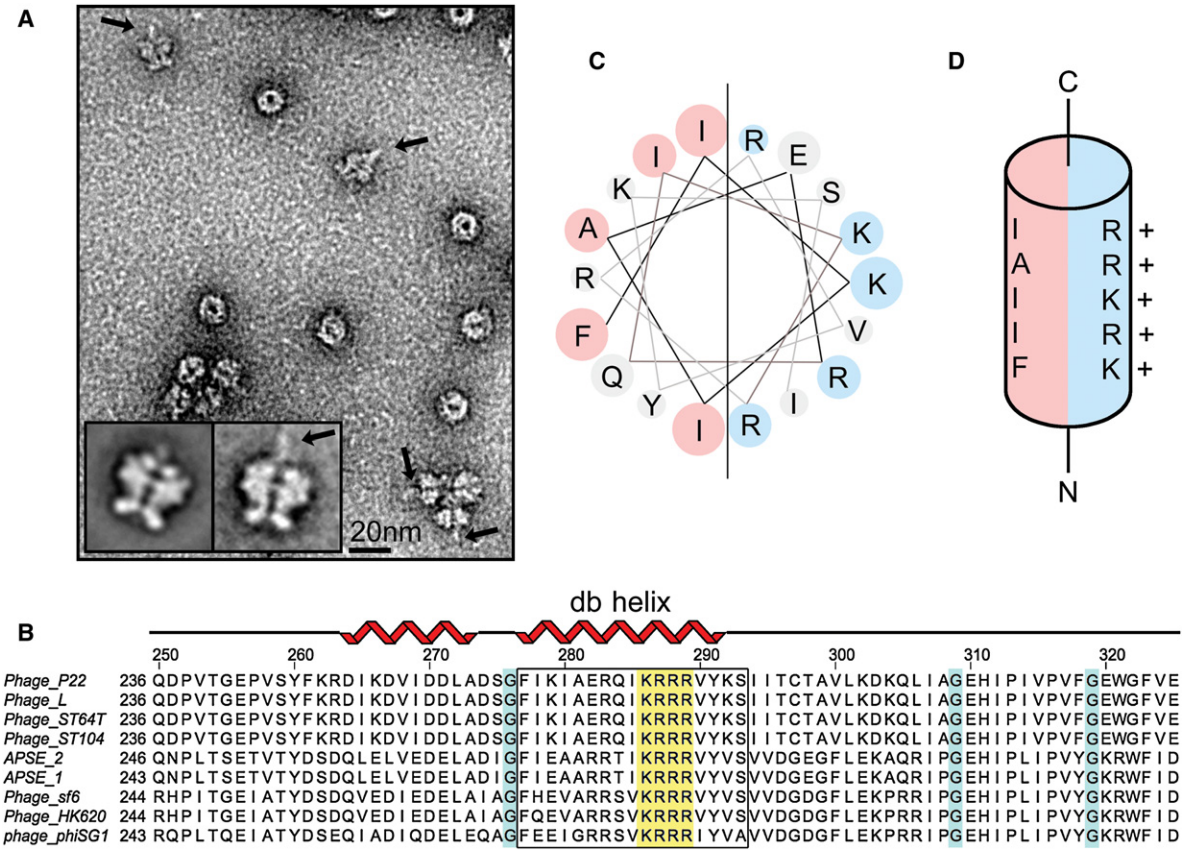

Figure 5. DNA Binding to Portal$_{602}$ Dome Domain

(A) Negatively stained preparation of portal$_{602}$:gp4 in complex with DNA. An elongated density (~100 Å) is clearly visible projecting outward from the dome domain of portal$_{602}$:gp4 in the presence of DNA (arrows). Inset projection averages: portal$_{602}$:gp4 on the left, DNA-bound portal$_{602}$:gp4 on the right.

(B) Sequence alignment of nine related portal proteins identify a possible DNA-binding helix (db helix). A stretch of conserved positively charged residues is identified in yellow. Surrounding glycine residues (highlighted in blue) suggest this region may be flexible.

(C and D) When folded as a helix, one face is positively charged and may be important for DNA binding, while the other face is hydrophobic and may be important for packing interactions. Multiple sequence alignment (Altschul et al., 1990) was done in Clustal W (Thompson et al., 1994); secondary structure prediction was performed with PREDATOR (Frishman and Argos, 1996) and helical wheel representation according to Schiffer and Edmundson (1967).

coiled conformation in solution (Cingolani et al., 2000) as well as in the autoinhibited structure of importin α (Kobe, 1999) but becomes folded into a helix upon binding to the acidic surface of the receptor importin β (Cingolani et al., 1999).

Virus Morphogenesis and Initiation of Infection

The 17 Å electron cryomicroscopy reconstruction of the mature P22 virion (Chang et al., 2006; Lander et al., 2006) shows a large DNA-filled icosahedral capsid (Figure 6A, gray), of which a unique 5-fold vertex is occupied by the genome injection machinery (Figure 6A, green). Four donut-like densities were identified directly above the portal protein and were postulated to be injection proteins (Lander et al., 2006). We extracted the density for the genome injection machinery together with the four densities and fit our portal$_{602}$:gp4 reconstruction (filtered to 17 Å resolution to facilitate the following comparison) into the full-length portal protein reconstruction from the mature virion (Lander et al., 2006) (Figures 6B and 6C). An overlay of the two reconstructions matches well: the dome domain seen in the portal$_{602}$:gp4 reconstruction clearly exists in the mature virion, and the C-terminal residues lacking in portal$_{602}$ clearly localize to these exterior spokes (Figure 6C, arrows). Although the dome forms a hollow donut surrounding genomic dsDNA in the mature virion (Lander et al., 2006), the very same region of the dome is solid in our portal$_{602}$:gp4 reconstruction (Figure 3).

In addition to binding DNA, the dome domain may be important in recruiting the injection proteins. This is supported by the cryomicroscopy reconstruction of the mature phage P22, in which three additional rings of density are visible above the dome domain, which are likely the injection proteins gp7, gp16, and gp20 (Lander et al., 2006). It is possible that, as genome packaging nears completion and the procapsid undergoes conformational changes to the mature capsid form, the terminase complex is displaced by gp4. The binding-induced oligomerization of gp4 (Olia et al., 2006) onto the funnel domain of the portal ring would initiate a global conformational switch in the portal protein that erects the dome domain directly above the DNA channel. This domain may function as a clamp to grasp

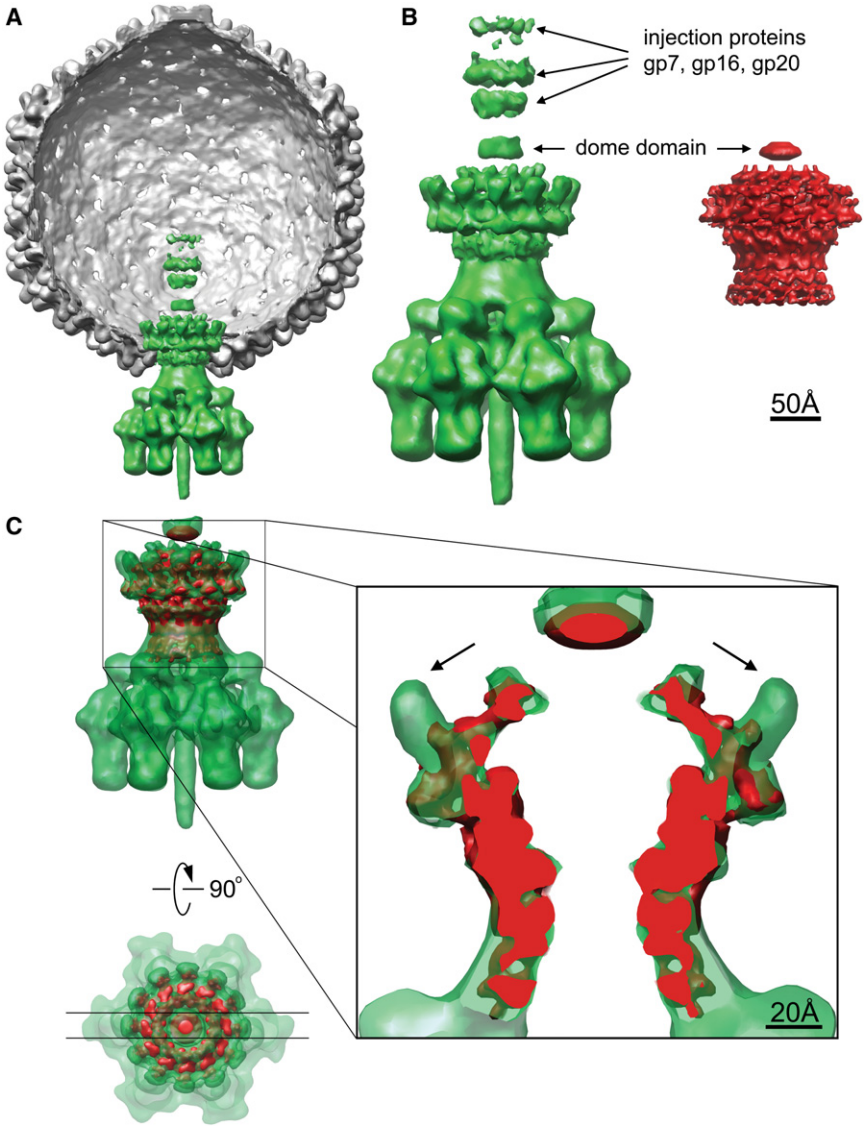

Figure 6. Mapping Portal$_{602}$:gp4 in the Mature P22 Virion

(A) Electron cryomicroscopy reconstruction of the mature P22 virion (MSD #1220). The capsid and the mature genome injection machinery are colored gray and green, respectively. For clarity, the DNA density has been removed from within the capsid.

(B) Scaled comparison of the genome injection machinery from mature P22 (green) and our portal$_{602}$:gp4 complex filtered to the same resolution to facilitate this comparison (red).

(C) Superposition of the two density maps reveals that the density above the portal protein in the mature phage corresponds to the dome domain seen in our reconstruction. The missing density of portal$_{602}$ is in the spokes (arrows). Additional rings of density above the dome domain may represent the injection proteins (Israel, 1977; Lander et al., 2006).

the dsDNA that still lines the channel and to recruit the injection proteins from within the virion, as seen in the mature phage cryoreconstruction (Lander et al., 2006). The arginine-rich stretch of the dome domain folds upon binding to the acidic DNA, forming a highly positively charged surface in the dome, used to prime DNA in preparation for a new round of viral infection.

Closing Remarks

Using electron cryomicroscopy, we have characterized a dramatic conformational change in the large portal protein of bacteriophage P22. Free portal$_{602}$, in its procapsid conformation, adopts a quaternary structure significantly different from that seen in the mature virion. We demonstrate that the conformational switch from the procapsid form to a mature phage conformation is specifically triggered by the assembly of tail factor gp4. When DNA packaging is complete, the terminase is disassembled from portal protein, likely via direct competition with the tail accessory factor gp4, which oligomerizes upon binding to the portal ring (Olia et al., 2006). This binding event, which marks the beginning of the tail assembly, leads to a dramatic reorganization of the DNA channel into its mature phage conformation, in which a dome-shaped domain is stabilized directly above the DNA channel. This domain functions as a DNA-binding scaffold, possibly used to clamp onto the viral genome and recruit the injection proteins at the portal protein vertex from inside the virion.

Our work provides an important snapshot of how the end of virus morphogenesis may be coupled to a new round of infection. In the context of the mature phage reconstruction (Chang et al., 2006; Lander et al., 2006), the gp4-induced conformational switch in portal protein may serve to recruit both viral DNA and the injection proteins in preparation for a new round of viral infection. Future studies must delve into the properties of the dome domain and its association with viral DNA and injection proteins. Similarly, investigation into maturation events in portal proteins from members of the herpesvirus family is critical for understanding how these viruses specifically release their genome into the cell nucleus upon interaction with the nuclear pore complex.

EXPERIMENTAL PROCEDURES

Expression, Purification, and Assembly of Dodecameric Portal Protein Complexes

The gene-encoding phage P22 portal protein (gp1) was cloned in a pET-21b vector. The C-terminal histidine tag was removed by site-directed mutagenesis by introducing a stop codon immediately after residue 725. C-terminally truncated portal protein (1–602) was generated by introducing an amber stop codon at position 603. Both untagged portal protein constructs were expressed in *E. coli* strain BL21 cells for 4–5 hr at 30°C and purified from the soluble fraction using 30% ammonium sulfate. Precipitated portal monomer

was dialyzed and concentrated to ~200 mg/ml using a Millipore 100 kDa concentrator. To enrich the sample for fully assembled dodecameric portal rings, 0.5 M EDTA was added to a final concentration of 60 mM, and portal protein samples were incubated at 37°C for 2–3 hr. The heat shock resulted in massive precipitation, which was pelleted by centrifuging at 100,000 × g for 35 min. The resulting supernatant, which contained only fully oligomerized dodecameric portal protein (Lorenzen et al., 2008), was further purified on a Sephacyl S-300 gel filtration column equilibrated with phosphate-buffered saline. Recombinant gp4 was expressed in *E. coli* strain BL21 cells and purified as described before (Olia et al., 2006). The complex $portal_{602}$:gp4 was formed by adding a 3-fold molar excess of gp4 to dodecameric portal protein followed by purification of the complex on a Sephacyl 300 gel filtration column. Native gel electrophoresis on agarose gel was performed according to established procedures (Olia et al., 2006). For DNA binding, $portal_{602}$ or $portal_{602}$:gp4 complexes were incubated with a 38 bp segment of DNA (sequence ACGGTTTCCCCGAAATTG ACGGATTTCCCCGAAATGGC). Preparations were negatively stained according to established protocols (Ohi et al., 2004) and viewed on a transmission electron microscope operated at 100 kv (Morgagni, FEI, Hillsboro, Oregon). Images were recorded using a 2k × 2k Gatan charge coupled device camera. Projection averages for both $portal_{602}$:gp4 and DNA-bound $portal_{602}$:gp4 were calculated in Spider (Frank et al., 1996).

Electron Cryomicroscopy and Data Processing

Full-length portal protein ($portal_{725}$), $portal_{602}$, and $portal_{602}$:gp4 complexes were prepared for electron cryomicroscopy as follows. A 2 μl drop of sample at 10 mg/ml was applied to a Quantifoil holey carbon grid (Quantifoil, Germany), blotted with filter paper, and immediately frozen in liquid ethane using a Vitrobot (FEI, Hillsboro, Oregon). Grids were mounted onto a Gatan high-resolution cryo holder and inserted into an FEI Tecnai F20 microscope equipped with a field emission gun and operated at 200 kv. Images of the vitrified specimen were recorded under low-dose conditions at a nominal magnification of 50,000× and defocus values ranging from 2.5 to 5 μm. All micrographs were visually examined using an optical diffractometer to select only drift-free images with no significant astigmatism. The film was digitized with a Nikon Super Cool Scan 9000 using a step size of 6.9 μm corresponding to 1.27 Å/pixel. Digitized micrographs were binned twice, yielding a pixel size of 2.54 Å. Approximately 20,000 individual particles were selected for $portal_{602}$, and 36,000 for $portal_{602}$:gp4 using WEB, and processed in SPIDER to generate an initial low-resolution 3D density map following established protocols (Frank et al., 1996). Image refinement using FREALIGN version 7.00 (Grigorieff, 2007) was performed as described previously (Fotin et al., 2004). Briefly, the contrast transfer function (CTF) parameters were determined for each micrograph using the program CTFTILT (Mindell and Grigorieff, 2003), and only those images where the CTF parameters could be accurately determined were used for further refinement. CTFTILT was used to calculate the defocus, astigmatism angle, position of tilt angle and tilt axis, and x and y coordinates for each individual particle from every usable micrograph. Search and refine protocols were used in FREALIGN (Grigorieff, 2007) and were limited initially to a resolution range of 500–40 Å. Euler angles and x, y shifts for each individual particle relative to the initial search model were determined and further refined in consecutive rounds of refinement in FREALIGN (Grigorieff, 2007). The nominal resolution of the final reconstruction was estimated from the spatial frequency at which the FSC fell to 0.143 (Rosenthal and Henderson, 2003) was 8 Å for $portal_{602}$ and 8.5 Å for $portal_{602}$:gp4 complex (Figure 1D). Both density maps were filtered to 10 Å resolution to facilitate the comparison, and a negative B factor of 1000 $Å^2$ was applied to the final reconstructions to restore high-resolution contrast. Density maps were normalized in MAPMAN version 7.8 (Kleywegt and Jones, 1996). The Contour sigma threshold was determined in Spider (Frank et al., 1996) and was 4.6σ above background for $portal_{602}$ (760 kDa) and 4.1σ above background for $portal_{602}$:gp4 (1.1 mDa). Density maps were visualized in UCSF Chimera (Pettersen et al., 2004) and all figures prepared using the above sigma levels. $Portal_{725}$ was reconstructed to 24 Å resolution and could not be further refined because of the lack of side views (De Rosier and Klug, 1968) (Figure 1A). $Portal_{602}$ and $portal_{602}$:gp4 were rotationally and translationally aligned in UCSF Chimera (Pettersen et al., 2004) until density features common to both lined up (Figure S3). Figure S4 shows the electron cryomicroscopy reconstructions for both $portal_{602}$ and $portal_{602}$:gp4, filtered to 12.5 and 12 Å, respectively, and corresponding to the spatial frequency at which the FSC fell to 0.5 (Stewart et al., 1999) (Figure S4). All features described in this manuscript are clearly visible using both 0.143 (Rosenthal and Henderson, 2003) and 0.5 (Stewart et al., 1999) FSC criteria.

Supplemental Data

Supplemental Data include four figures and can be found with this article online at http://www.molecule.org/cgi/content/full/29/3/376/DC1/.

ACKNOWLEDGMENTS

The authors thank Bridget Carragher and Clinton Potter (Scripps, La Jolla, CA) for allowing us to use their electron cryomicroscopes for data collection. Electron micrographs were collected at the National Resource for Automated Molecular Microscopy (NRAMM), which is supported by the National Institutes of Health though the National Center for Research Resources' P41 program (RR17573). We would also like to thank Thomas Walz (Harvard Medical School) for the use of his electron cryomicroscope in the early stages of this study. The authors thank Yifan Cheng (University of California, San Francisco) for helpful discussions about single-particle reconstructions and Sherwood Casjens (University of Utah) and Carlos Catalano (University of Washington) for helpful discussions on bacteriophage P22. The authors declare that none have financial interests related to this work. H.Z., M.G., S.A., and T.G. collected the electron cryomicroscopy data, did all the data processing and subsequent analysis, and prepared manuscript figures. A.S.O. and G.C. prepared the $portal_{725}$, $portal_{602}$, and $portal_{602}$:gp4 complexes and did the gel shift assay. G.C. and T.G. wrote the manuscript.

Received: July 30, 2007
Revised: October 8, 2007
Accepted: November 16, 2007
Published: February 14, 2008

REFERENCES

Agirrezabala, X., Martin-Benito, J., Valle, M., Gonzalez, J.M., Valencia, A., Valpuesta, J.M., and Carrascosa, J.L. (2005). Structure of the connector of bacteriophage T7 at 8 Å resolution: structural homologies of a basic component of a DNA translocating machinery. J. Mol. Biol. *347*, 895–902.

Altschul, S.F., Gish, W., Miller, W., Myers, E.W., and Lipman, D.J. (1990). Basic local alignment search tool. J. Mol. Biol. *215*, 403–410.

Bazinet, C., Villafane, R., and King, J. (1990). Novel second-site suppression of a cold-sensitive defect in phage P22 procapsid assembly. J. Mol. Biol. *216*, 701–716.

Bhardwaj, A., Olia, A.S., Walker-Kopp, N., and Cingolani, G. (2007). Domain organization and polarity of tail needle gp26 in the portal vertex structure of bacteriophage P22. J. Mol. Biol. *371*, 374–387.

Casjens, S., and Huang, W.M. (1982). Initiation of sequential packaging of bacteriophage P22 DNA. J. Mol. Biol. *157*, 287–298.

Chang, J., Weigele, P., King, J., Chiu, W., and Jiang, W. (2006). Cryo-EM asymmetric reconstruction of bacteriophage P22 reveals organization of its DNA packaging and infecting machinery. Structure *14*, 1073–1082.

Chemla, Y.R., Aathavan, K., Michaelis, J., Grimes, S., Jardine, P.J., Anderson, D.L., and Bustamante, C. (2005). Mechanism of force generation of a viral DNA packaging motor. Cell *122*, 683–692.

Cingolani, G., Petosa, C., Weis, K., and Muller, C.W. (1999). Structure of importin-beta bound to the IBB domain of importin-alpha. Nature *399*, 221–229.

Cingolani, G., Lashuel, H.A., Gerace, L., and Muller, C.W. (2000). Nuclear import factors importin alpha and importin beta undergo mutually induced conformational changes upon association. FEBS Lett. *484*, 291–298.

Cingolani, G., Moore, S.D., Prevelige, P.E., Jr., and Johnson, J.E. (2002). Preliminary crystallographic analysis of the bacteriophage P22 portal protein. J. Struct. Biol. *139*, 46–54.

De Rosier, D.J., and Klug, A. (1968). Reconstruction of three dimensional structures from electron micrographs. Nature *217*, 130–134.

Earnshaw, W.C., and Harrison, S.C. (1977). DNA arrangement in isometric phage heads. Nature *268*, 598–602.

Earnshaw, W.C., King, J., Harrison, S.C., and Eiserling, F.A. (1978). The structural organization of DNA packaged within the heads of T4 wild-type, isometric, and giant bacteriophages. Cell *14*, 559–568.

Fotin, A., Cheng, Y., Sliz, P., Grigorieff, N., Harrison, S.C., Kirchhausen, T., and Walz, T. (2004). Molecular model for a complete clathrin lattice from electron cryomicroscopy. Nature *432*, 573–579.

Frank, J., Radermacher, M., Penczek, P., Zhu, J., Li, Y., Ladjadj, M., and Leith, A. (1996). SPIDER and WEB: processing and visualization of images in 3D electron microscopy and related fields. J. Struct. Biol. *116*, 190–199.

Frishman, D., and Argos, P. (1996). Incorporation of non-local interactions in protein secondary structure prediction from the amino acid sequence. Protein Eng. *9*, 133–142.

Grigorieff, N. (2007). FREALIGN: high-resolution refinement of single particle structures. J. Struct. Biol. *157*, 117–125.

Guasch, A., Pous, J., Parraga, A., Valpuesta, J.M., Carrascosa, J.L., and Coll, M. (1998). Crystallographic analysis reveals the 12-fold symmetry of the bacteriophage phi29 connector particle. J. Mol. Biol. *281*, 219–225.

Israel, V. (1977). E proteins of bacteriophage P22. I. Identification and ejection from wild-type and defective particles. J. Virol. *23*, 91–97.

Ivanovska, I.L., de Pablo, P.J., Ibarra, B., Sgalari, G., MacKintosh, F.C., Carrascosa, J.L., Schmidt, C.F., and Wuite, G.J. (2004). Bacteriophage capsids: tough nanoshells with complex elastic properties. Proc. Natl. Acad. Sci. USA *101*, 7600–7605.

Jackson, E.N., Laski, F., and Andres, C. (1982). Bacteriophage P22 mutants that alter the specificity of DNA packaging. J. Mol. Biol. *154*, 551–563.

Jiang, W., Li, Z., Zhang, Z., Baker, M.L., Prevelige, P.E., Jr., and Chiu, W. (2003). Coat protein fold and maturation transition of bacteriophage P22 seen at subnanometer resolutions. Nat. Struct. Biol. *10*, 131–135.

Johnson, J.E., and Chiu, W. (2007). DNA packaging and delivery machines in tailed bacteriophages. Curr. Opin. Struct. Biol. *17*, 237–243.

Kleywegt, G.J., and Jones, T.A. (1996). xdlMAPMAN and xdlDATAMAN—programs for reformatting, analysis and manipulation of biomacromolecular electron-density maps and reflection data sets. Acta Crystallogr. D Biol. Crystallogr. *52*, 826–828.

Knopf, C.W. (2000). Molecular mechanisms of replication of herpes simplex virus 1. Acta Virol. *44*, 289–307.

Kobe, B. (1999). Autoinhibition by an internal nuclear localization signal revealed by the crystal structure of mammalian importin alpha. Nat. Struct. Biol. *6*, 388–397.

Lander, G.C., Tang, L., Casjens, S.R., Gilcrease, E.B., Prevelige, P., Poliakov, A., Potter, C.S., Carragher, B., and Johnson, J.E. (2006). The structure of an infectious p22 virion shows the signal for headful DNA packaging. Science *312*, 1791–1795.

Lorenzen, K., Olia, A.S., Uetrecht, C., Cingolani, G., and Heck, A.J.R. (2008). Structural effects of gp4 assembly to phage P22 portal protein. J. Mol. Biol., in press.

Mettenleiter, T.C., Klupp, B.G., and Granzow, H. (2006). Herpesvirus assembly: a tale of two membranes. Curr. Opin. Microbiol. *9*, 423–429.

Mindell, J.A., and Grigorieff, N. (2003). Accurate determination of local defocus and specimen tilt in electron microscopy. J. Struct. Biol. *142*, 334–347.

Newcomb, W.W., Juhas, R.M., Thomsen, D.R., Homa, F.L., Burch, A.D., Weller, S.K., and Brown, J.C. (2001). The UL6 gene product forms the portal for entry of DNA into the herpes simplex virus capsid. J. Virol. *75*, 10923–10932.

Ohi, M., Li, Y., Cheng, Y., and Walz, T. (2004). Negative staining and image classification—powerful tools in modern electron microscopy. Biol. Proced. Online *6*, 23–34.

Olia, A.S., Al-Bassam, J., Winn-Stapley, D.A., Joss, L., Casjens, S.R., and Cingolani, G. (2006). Binding-induced stabilization and assembly of the phage P22 tail accessory factor gp4. J. Mol. Biol. *363*, 558–576.

Orlova, E.V., Gowen, B., Droge, A., Stiege, A., Weise, F., Lurz, R., van Heel, M., and Tavares, P. (2003). Structure of a viral DNA gatekeeper at 10 Å resolution by cryo-electron microscopy. EMBO J. *22*, 1255–1262.

Pettersen, E.F., Goddard, T.D., Huang, C.C., Couch, G.S., Greenblatt, D.M., Meng, E.C., and Ferrin, T.E. (2004). UCSF Chimera—a visualization system for exploratory research and analysis. J. Comput. Chem. *25*, 1605–1612.

Poliakov, A., van Duijn, E., Lander, G., Fu, C.Y., Johnson, J.E., Prevelige, P.E., Jr., and Heck, A.J. (2007). Macromolecular mass spectrometry and electron microscopy as complementary tools for investigation of the heterogeneity of bacteriophage portal assemblies. J. Struct. Biol. *157*, 371–383.

Rosenthal, P.B., and Henderson, R. (2003). Optimal determination of particle orientation, absolute hand, and contrast loss in single-particle electron cryomicroscopy. J. Mol. Biol. *333*, 721–745.

Schiffer, M., and Edmundson, A.B. (1967). Use of helical wheels to represent the structures of proteins and to identify segments with helical potential. Biophys. J. *7*, 121–135.

Simpson, A.A., Tao, Y., Leiman, P.G., Badasso, M.O., He, Y., Jardine, P.J., Olson, N.H., Morais, M.C., Grimes, S., Anderson, D.L., et al. (2000). Structure of the bacteriophage phi29 DNA packaging motor. Nature *408*, 745–750.

Simpson, A.A., Leiman, P.G., Tao, Y., He, Y., Badasso, M.O., Jardine, P.J., Anderson, D.L., and Rossmann, M.G. (2001). Structure determination of the head-tail connector of bacteriophage phi29. Acta Crystallogr. D Biol. Crystallogr. *57*, 1260–1269.

Steven, A.C., Trus, B.L., Booy, F.P., Cheng, N., Zlotnick, A., Caston, J.R., and Conway, J.F. (1997). The making and breaking of symmetry in virus capsid assembly: glimpses of capsid biology from cryoelectron microscopy. FASEB J. *11*, 733–742.

Stewart, P.L., Chiu, C.Y., Haley, D.A., Kong, L.B., and Schlessman, J.L. (1999). Review: resolution issues in single-particle reconstruction. J. Struct. Biol. *128*, 58–64.

Strauss, H., and King, J. (1984). Steps in the stabilization of newly packaged DNA during phage P22 morphogenesis. J. Mol. Biol. *172*, 523–543.

Thompson, J.D., Higgins, D.G., and Gibson, T.J. (1994). CLUSTAL W: improving the sensitivity of progressive multiple sequence alignment through sequence weighting, position-specific gap penalties and weight matrix choice. Nucleic Acids Res. *22*, 4673–4680.

Thuman-Commike, P.A., Greene, B., Jakana, J., Prasad, B.V., King, J., Prevelige, P.E., Jr., and Chiu, W. (1996). Three-dimensional structure of scaffolding-containing phage p22 procapsids by electron cryo-microscopy. J. Mol. Biol. *260*, 85–98.

Trus, B.L., Cheng, N., Newcomb, W.W., Homa, F.L., Brown, J.C., and Steven, A.C. (2004). Structure and polymorphism of the UL6 portal protein of herpes simplex virus type 1. J. Virol. *78*, 12668–12671.

Ye, X., Gorin, A., Ellington, A.D., and Patel, D.J. (1996). Deep penetration of an alpha-helix into a widened RNA major groove in the HIV-1 rev peptide-RNA aptamer complex. Nat. Struct. Biol. *3*, 1026–1033.

Ye, X., Gorin, A., Frederick, R., Hu, W., Majumdar, A., Xu, W., McLendon, G., Ellington, A., and Patel, D.J. (1999). RNA architecture dictates the conformations of a bound peptide. Chem. Biol. *6*, 657–669.

Zhang, Z., Greene, B., Thuman-Commike, P.A., Jakana, J., Prevelige, P.E., Jr., King, J., and Chiu, W. (2000). Visualization of the maturation transition in bacteriophage P22 by electron cryomicroscopy. J. Mol. Biol. *297*, 615–626.

Accession Numbers

Density maps portal$_{725}$, portal$_{602}$, and portal$_{602}$:gp4 have been deposited at the Macromolecular Structure Database under reference numbers 5631, 5632, and 5633, respectively.